Polaron properties of III-V nitride compounds: second-order effects

1999 J. Phys.: Condens. Matter 11 8223

(http://iopscience.iop.org/0953-8984/11/42/304)

J. Phys.: Condens. Matter **11** (1999) 8223–8238. Printed in the UK PII: S0953-8984(99)02593-X

Polaron properties of III–V nitride compounds: second-order effects

M E Mora-Ramos†§, F J Rodríguez‡ and L Quiroga‡

† Facultad de Ciencias, Universidad Autónoma del Estado de Morelos, Avenida Universidad 1001, CP 62210, Cuernavaca, Morelos, Mexico
‡ Departamento de Física, Universidad de Los Andes, AA 4976, Santafé de Bogotá, Colombia

E-mail: memora@servm.fc.uaem.mx

Received 15 March 1999, in final form 5 August 1999

Abstract. The polaron binding energy and effective mass are obtained for bulk III–V nitride compounds with wurtzite crystalline structure with the use of a recently derived dielectric continuum Fröhlich-like electron–phonon interaction Hamiltonian which accounts for the mixing of the longitudinal optical and transverse optical polarization due to the anisotropy. Corrections are calculated up to second order in the coupling constants. Numerical results are reported for GaN and AlN. Good quantitative agreement with experimental results for the electronic effective mass is obtained for GaN.

1. Introduction

Electronics and optoelectronics based on III–V wide-band-gap nitride semiconducting systems have emerged as subjects of particular interest in recent years. GaN and its alloys with Al and In exhibit high thermal conductivity and stability, and are thus ideally suited for use in making optoelectronic devices operating at room temperature. GaN-based light-emitting diodes, lasers, and detectors working in the visible-to-ultraviolet range have been built, as well as high-power transistors with operating frequencies in the microwave region (Khan *et al* 1993, 1995, Nakamura *et al* 1994, 1996, 1997, van de Walle 1993, Moustakas *et al* 1992, Dupuis *et al* 1996, Ponce *et al* 1997). On the other hand, wurtzite InN seems to have considerable potential for device applications due to its transport characteristics—a very high peak and saturation drift velocities—which are better than those of gallium nitride and gallium arsenide, over a wide range of temperatures, and high doping concentrations (O'Leary *et al* 1998).

Under ambient conditions, III–V nitrides have the wurtzite structure. However, at high pressure some of them, e.g. GaN and AlN, have been known to undergo a structural phase transition to a rock-salt structure. The electronic properties of both the hexagonal and the cubic structures have been investigated in detail using a local-density-functional formalism (Van Camp *et al* 1991, 1992). Nitrides exhibit highly unusual properties among the III–V group of semiconductors, resembling more, in some respects, the II–VI compounds. In particular, they present large spontaneous and piezoelectric polarizations (Bernardini *et al* 1997).

Over the past few years there has been great interest in carrier–optical-phonon interaction in polar semiconductors. Recently, the electron–phonon interaction mechanism in crystals

§ Author to whom any correspondence should be addressed. Fax: (52)(73) 297040.

with wurtzite structure has been considered. A new Fröhlich-type electron–phonon model Hamiltonian has been put forward for the bulk case (Lee *et al* 1997), and for wurtzite single and double heterostructures (Lee *et al* 1998), within the non-retarded Born–Huang dielectric continuum model (DCM).

It is known that the DCM describes the optical-phonon modes in bulk ionic crystals very well in a macroscopic continuum approximation. However, it fails to correctly describe the mechanical part of the oscillation field in systems with interfaces, thus being unable to reproduce the results from Raman spectra (Trallero-Giner *et al* 1992, Ridley 1993). The treatment in this work will be restricted to bulk systems.

In the proposed DCM model of Lee *et al* (1997), only the three optical-phonon branches which are infrared active in the wurtzite structure are considered. Probably the most important result arising from that work is the mixing of the longitudinal optical (LO) and transverse optical (TO) modes due to the lattice anisotropy. As a consequence, both kinds of mode should significantly contribute to the carrier scattering. A similar behaviour is well known in semiconducting heterostructures, where the presence of interfaces breaks the isotropy in one or more spatial directions, leading to the mixing of the longitudinal and transverse oscillation polarizations (Comas *et al* 1993, 1997), and all of them have to be included in the study of the electron–phonon interaction because even the TO-type modes can provide a non-negligible contribution (Mora-Ramos and Contreras-Solorio 1998) to the scattering rates and polaron properties.

Furthermore, the existence of a spatial direction with low symmetry (the z-axis) also gives rise to phonon dispersion. To illustrate this, let us mention the application of the macroscopic DCM to the study of the long-wavelength optical oscillations in dielectric or semiconducting heterolayers (Wendler 1985). In that case, even when no phonon dispersion is considered for the bulk constituent materials, the dispersion law $\omega(q)$ is typical for the so-called interface modes. For wurtzite III–V nitrides, phonon dispersion effects should be expected. In fact, the dependence of the oscillation frequencies upon the phonon wavevector $\boldsymbol{q}$ is a function not of the wavevector magnitude but of the angle between $\boldsymbol{q}$ and the z-axis of the structure (Lee *et al* 1997).

Electron–optical-phonon interaction is one of the major scattering mechanisms limiting the carrier mobility, and also plays an important role in the study of optical properties in ionic crystals. The electron–phonon scattering rates calculated with the use of the above-mentioned Hamiltonian (Lee *et al* 1997) are sufficiently large to indicate a rather strong interaction, and to motivate the study of the polaronic corrections to the energy and the effective mass of slow electrons in the conduction band of wurtzite nitride materials.

The polaron is a quasiparticle state consisting of an electron and its surrounding phonon cloud (Fröhlich 1954). When electrons move through a polar material, they polarize the surrounding medium and couple to the self-induced polarization field (Davydov 1976). This coupling acts as some kind of drag that slows down the electron, as it acquires an additional mass, and—at the same time—behaves as a potential well, decreasing its zero-momentum energy, and thus tending to localize the electron (which is what actually happens when the coupling is strong enough). Even for weakly polar materials, these corrections may be quite important. For information about the state of the art on polaron theory in polar semiconductors and dielectrics and a thorough discussion of both the weak- and strong-coupling polaron regimes, see the review by Devreese (1996).

In a previous paper we presented the results for polaronic corrections to the binding energy and effective mass, evaluated from first-order Rayleigh–Schrödinger perturbation theory for the case of wurtzite GaN (Mora-Ramos *et al* 1999), showing that the magnitude of the correction is, in each case, high enough for us to expect a non-negligible contribution to arise from

the second-order terms in the self-energy perturbation expansion. Thus, looking for a more realistic value of the polaronic corrections, calculations up to the second perturbative order in the coupling constants have to be carried out. In the present work, polaron calculations are performed for bulk wurtzite nitride materials along the lines of the dielectric long-wavelength continuum model of Lee *et al* (1997); we report both first- and second-order contributions. The importance of the second-order corrections is revealed and commented on.

The paper is organized as follows. In section 2, the results from the DCM for the interaction Hamiltonian are reviewed. Section 3 contains the details of the calculation of the polaronic corrections. In section 4, numerical values for the polaron binding energy and effective mass are presented and discussed for the particular cases of GaN and AlN. Finally, the results are summarized in the conclusions (section 5).

2. The interaction Hamiltonian

In the framework of the non-retarded DCM, the electron–phonon interaction Hamiltonian corresponding to the infrared-active phonon frequencies of wurtzite structures is written as the sum of two contributions, i.e.

$$\hat{H}_{\mathrm{e-ph}} = \hat{H}_{\mathrm{e-LO}} + \hat{H}_{\mathrm{e-TO}} \tag{1}$$

where $\hat{H}_{\mathrm{e-LO}}$ and $\hat{H}_{\mathrm{e-TO}}$ stand, respectively, for the electron–LO-like-phonon interaction and the electron–TO-like-phonon interaction. Both Hamiltonians have the usual Fröhlich-like form and the electron–phonon vertices are given, respectively, by (Lee *et al* 1997)

$$|M_{\boldsymbol{q}}^{\mathrm{L}}|^2 = \frac{2\pi e^2\overline{h}}{Vq^2\Omega_{\mathrm{L}}}\left[\frac{\sin^2\theta}{(1/\epsilon_{\perp}^{*})\omega_{\perp\mathrm{L}}^2} + \frac{\cos^2\theta}{(1/\epsilon_{z}^{*})\omega_{z\mathrm{L}}^2}\right]^{-1} \tag{2}$$

and

$$|M_{\boldsymbol{q}}^{\mathrm{T}}|^2 = \frac{2\pi e^2\overline{h}}{Vq^2\Omega_{\mathrm{T}}}\frac{(\omega_{\perp}^2-\omega_{z}^2)^2\sin^2\theta\cos^2\theta}{(\epsilon_{\perp}^{0}-\epsilon_{\perp}^{\infty})\omega_{\perp}^2\cos^2\theta + (\epsilon_{z}^{0}-\epsilon_{z}^{\infty})\omega_{z}^2\sin^2\theta}. \tag{3}$$

Here,

$$1/\epsilon_{\perp}^{*} = 1/\epsilon_{\perp}^{\infty} - 1/\epsilon_{\perp}^{0} \qquad \text{and} \qquad 1/\epsilon_{z}^{*} = 1/\epsilon_{z}^{\infty} - 1/\epsilon_{z}^{0}$$

where $\epsilon_{\perp}^{\infty}$ (ϵ_{z}^{∞}) is the high-frequency dielectric constant perpendicular to (along) the z-axis, and

$$\epsilon_{\perp}^{0} = \epsilon_{\perp}^{\infty}\omega_{\perp\mathrm{L}}^2/\omega_{\perp}^2 \qquad \text{and} \qquad \epsilon_{z}^{0} = \epsilon_{z}^{\infty}\omega_{z\mathrm{L}}^2/\omega_{z}^2$$

are the static dielectric constants. $\omega_{z\mathrm{L}}$ and $\omega_{\perp\mathrm{L}}$ are the LO-phonon frequencies along and perpendicular to the z-axis respectively, and ω_z and $\omega_{\perp}$ are the corresponding lattice dispersion frequencies. For simplicity, ϵ_{z}^{∞} and $\epsilon_{\perp}^{\infty}$ are assumed to be equal. The characteristic frequencies Ω_{L} and Ω_{T} are also functions of θ, the angle between the wavevector $\boldsymbol{q}$ and the z-axis. They are

$$\begin{aligned}\Omega_{\mathrm{L}}^2 &= \omega_{z\mathrm{L}}^2\cos^2\theta + \omega_{\perp\mathrm{L}}^2\sin^2\theta\\ \Omega_{\mathrm{T}}^2 &= \omega_{z}^2\sin^2\theta + \omega_{\perp}^2\cos^2\theta.\end{aligned} \tag{4}$$

Unlike the case for isotropic materials, the TO-like vertex $M_{\boldsymbol{q}}^{\mathrm{T}}$ is, in general, different from zero due to the polarization mixing. For instance, a pure transverse mode is obtained for $\theta = \pi/2$.

The electronic states are described, as usual, within the effective-mass approximation: the electron wavevector $\boldsymbol{k}$ is the quantum number which labels the state with energy $E = \overline{h}^2k^2/2m^*$

in the conduction band, which, for simplicity, is assumed to be spherically symmetric with an effective mass m^* (Lee *et al* 1997).

To deal with the entire range of θ, a Fröhlich-like coupling constant $\alpha_{\rm L}$ will be introduced through

$$\alpha_{\rm L}^2 = m^* e^4/(2\epsilon_\perp^* \epsilon_z^* \overline{h}^3 \omega_{\rm L})$$

where $\omega_{\rm L}$ is an 'effective longitudinal frequency'. In our case, we take $\omega_{\rm L} = \Omega_{\rm L}(\theta = \pi/4)$ to treat contributions coming from $\omega_{\perp{\rm L}}$ and $\omega_{z{\rm L}}$ on an equal footing (Mora-Ramos *et al* 1999). Then, an 'effective-longitudinal-polaron radius' $\rho_{\rm L}$ can be introduced through $\rho_{\rm L}^2 = \overline{h}/2m^*\omega_{\rm L}$.

Owing to our wish to describe the electron–TO-like-phonon interaction in terms of a certain dimensionless coupling parameter, we introduce another Fröhlich-like constant $\alpha_{\rm T}$, such that

$$\alpha_{\rm T}^2 = m^* e^4/(2\epsilon_\perp^* \epsilon_z^* \overline{h}^3 \omega_{\rm T})$$

(Mora-Ramos *et al* 1999). By the same arguments as were used to introduce the frequency $\omega_{\rm L}$, the 'effective transverse frequency' $\omega_{\rm T}$ is chosen to be $\omega_{\rm T} = \Omega_{\rm T}(\theta = \pi/4)$, and an 'effective-transverse-polaron radius' $\rho_{\rm T}$ is defined through $\rho_{\rm T}^2 = \overline{h}/2m^*\omega_{\rm T}$.

Now, the longitudinal and transverse electron–phonon vertices given in equations (2) and (3) are modified in the following way: the factor $2\pi e^2 \overline{h}$ is changed to

$$4\pi \overline{h}^2 \alpha_{\rm L}((1/\epsilon_z^*)(1/\epsilon_\perp^*))^{-1/2} \rho_{\rm L} \omega_{\rm L}$$

for the longitudinal case and to

$$4\pi \overline{h}^2 \alpha_{\rm T}((1/\epsilon_z^*)(1/\epsilon_\perp^*))^{-1/2} \rho_{\rm T} \omega_{\rm T}$$

for the transverse case. This way of choosing $\omega_{\rm L}$, $\omega_{\rm T}$, $\alpha_{\rm L}$, and $\alpha_{\rm T}$ to represent the electron–phonon interaction for the wurtzite is, of course, not unique. It is possible to follow different criteria; but what remains clear is that the final numerical results will be the same. Indeed, it makes no sense to compare the strengths of the electron–LO-like-phonon interaction and of the electron–TO-like-phonon interaction through the values of $\alpha_{\rm L}$ and $\alpha_{\rm T}$. However, both $\alpha_{\rm L}$ and $\alpha_{\rm T}$ could be representative values if comparisons between the strengths of the corresponding interactions for different wurtzite materials are made.

3. Polaronic corrections

As usual, the starting expression for the evaluation of the first-order perturbative polaronic corrections will be the real part of the electron self-energy in the one-particle limit at $T = 0$ K (Mahan 1990):

$$\Sigma_{\rm S}^{(1)}(k,\gamma,\eta) = -\frac{m^*}{\pi^2}\alpha_{\rm S}\rho_{\rm S}\omega_{\rm S}(\epsilon_z^*\epsilon_\perp^*)^{1/2} \times \int_0^\infty {\rm d}q \int_0^{2\pi} {\rm d}\varphi \int_{-1}^1 {\rm d}x \, \frac{f_{\rm S}(x)}{\Omega_{\rm S}(x)(q^2 - 2qk\cos\nu + 2m^*\Omega_{\rm S}(x)/\overline{h})} \tag{5}$$

where ${\rm S} = \{{\rm L}, {\rm T}\}$, $x = \cos\theta$, $\cos\nu = \cos(\varphi - \gamma)\sin\eta(1 - x^2)^{1/2} + x\cos\eta$, ν is the angle between the wavevectors $\boldsymbol{k}$ and $\boldsymbol{q}$, and (η, γ) denote the direction of $\boldsymbol{k}$. The characteristic phonon frequencies are then written as (Mora-Ramos *et al* 1999)

$$\Omega_{\rm S}^2(x) = \begin{cases} (\omega_{z{\rm L}}^2 - \omega_{\perp{\rm L}}^2)x^2 + \omega_{\perp{\rm L}}^2 & {\rm S} = {\rm L} \\ (\omega_\perp^2 - \omega_z^2)x^2 + \omega_z^2 & {\rm S} = {\rm T} \end{cases} \tag{6}$$

and

$$f_{\rm S}(x) = \begin{cases} \left[\dfrac{1-x^2}{(1/\epsilon_\perp^*)\omega_{\perp L}^2} + \dfrac{x^2}{(1/\epsilon_z^*)\omega_{z\rm L}^2} \right]^{-1} & {\rm S} = {\rm L} \\ \dfrac{(\omega_\perp^2 - \omega_z^2)^2 x^2 (1-x^2)}{(\epsilon_\perp^0 - \epsilon_\perp^\infty)\omega_\perp^2 x^2 + (\epsilon_z^0 - \epsilon_z^\infty)\omega_z^2 (1-x^2)} & {\rm S} = {\rm T}. \end{cases} \tag{7}$$

The integrand is expanded in powers of k—the electron wavevector magnitude—and only the terms up to second order are kept. Isotropy in the xy-plane eliminates any dependence on γ. Hence, the first-order polaron binding energy will be given by (Mora-Ramos *et al* 1999)

$$\varepsilon_{\rm p}^{(1)} = -\sum_{\rm S=L,T} \alpha_{\rm S} \xi_{\rm S}^{(1)} \hbar\omega_{\rm S} \tag{8}$$

where

$$\xi_{\rm S}^{(1)} = \left(\frac{\epsilon_z^* \epsilon_\perp^*}{\omega_{\rm S}} \right)^{1/2} \int_0^1 \frac{f_{\rm S}(x)}{\Omega_{\rm S}^{3/2}(x)}\, {\rm d}x. \tag{9}$$

On the other hand, the polaron mass is given by

$$m_{\rm p} = \frac{1}{1-\mu_{\rm p}(\eta)} \tag{10}$$

and the correction up to first order is given by

$$\mu_{\rm p}^{(1)}(\eta) = \sum_{\rm S=L,T} \alpha_{\rm S} \mu_{1\rm S}^{(1)} \cos^2\eta + \sum_{\rm S=L,T} \alpha_{\rm S} \mu_{2\rm S}^{(1)} \sin^2\eta. \tag{11}$$

The expressions for the quantities $\xi_{\rm S}^{(1)}$ and $\mu_{\rm S}^{(1)}$ are the following:

$$\mu_{1\rm S}^{(1)} = \frac{1}{2}(\omega_{\rm S}\epsilon_z^*\epsilon_\perp^*)^{1/2} \int_0^1 x^2 \frac{f_{\rm S}(x)}{\Omega_{\rm S}^{5/2}(x)}\, {\rm d}x \tag{12}$$

$$\mu_{2\rm S}^{(1)} = \frac{1}{4}(\omega_{\rm S}\epsilon_z^*\epsilon_\perp^*)^{1/2} \int_0^1 (1-x^2) \frac{f_{\rm S}(x)}{\Omega_{\rm S}^{5/2}(x)}\, {\rm d}x. \tag{13}$$

The second-order corrections to the polaron binding energy and effective mass are evaluated from the contributions of the diagrams depicted in figure 1. Since the electron–phonon Hamiltonian (1) contains two different interactions, each corresponding to a different polarization, there are, in fact, several diagrams with a particular topology. They are:

- One (a) diagram and one (b) diagram both with LO-like phonon lines (*case A*).
- One (a) diagram and one (b) diagram both with TO-like phonon lines (*case B*).
- Two (a) diagrams each with one LO-like phonon line plus one TO-like phonon line: the first one with an upper LO-like line (lower TO-like line) and the second one with an upper TO-like line (lower LO-like line) (*case C*).
- Two (b) diagrams each with one LO-like and one TO-like (crossed) phonon lines (*case D*).

Taking as the starting point the usual equations associated with second-order self-energy diagrams in the limits of zero temperature and one particle (Mahan 1990), and expanding the integrands up to second order in k, the resulting expressions for the polaron properties are obtained.

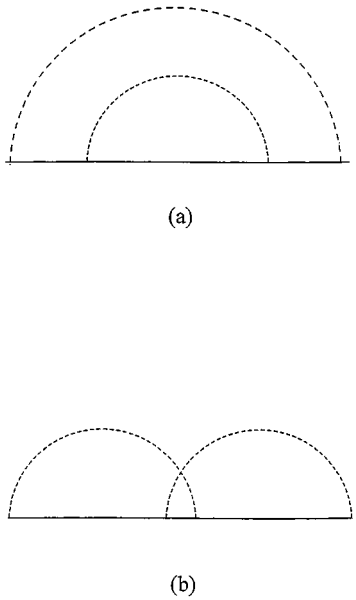

Figure 1. Second-order electron–phonon self-energy diagrams.

(i) *Cases A and B.* The contribution from the diagram of figure 1(a) with two SO-like phonon lines (S = {L, T}) will be

$$\Sigma^{(2)}_{\mathrm{S(a)}}(k,\eta) = -\alpha_{\mathrm{S}}^2\hbar\omega_{\mathrm{S}}\xi^{(2)}_{\mathrm{S(a)}} - \alpha_{\mathrm{S}}^2\frac{\hbar^2k^2}{2m^*}(\mu^{(2)}_{\mathrm{1S(a)}}\cos^2\eta + \mu^{(2)}_{\mathrm{2S(a)}}\sin^2\eta). \quad (14)$$

The contribution from the diagram of figure 1(b) with two SO-like phonon lines (S = {L, T}) is given by

$$\Sigma^{2}_{\mathrm{S(b)}}(k,\eta) = -\alpha_{\mathrm{S}}^2\hbar\omega_{\mathrm{S}}\xi^{(2)}_{\mathrm{S(b)}} - \alpha_{\mathrm{S}}^2\frac{\hbar^2k^2}{2m^*}(\mu^{(2)}_{\mathrm{1S(b)}}\cos^2\eta + \mu^{(2)}_{\mathrm{2S(b)}}\sin^2\eta). \quad (15)$$

(ii) *Case C.* To deal with those diagrams with phonon lines of different polarizations, a frequency $\bar{\omega} = \sqrt{\omega_{\mathrm{L}}\omega_{\mathrm{T}}}$ will be introduced. The diagram with an upper LO-like line contributes with

$$\Sigma^{(2)}_{\mathrm{SS'(a)}}(k,\eta) = -\alpha_{\mathrm{S}}\alpha_{\mathrm{S'}}\hbar\bar{\omega}\xi^{(2)}_{\mathrm{SS'(a)}} - \alpha_{\mathrm{S}}\alpha_{\mathrm{S'}}\frac{\hbar^2k^2}{2m^*}(\mu^{(2)}_{\mathrm{SS'(a)}}\cos^2\eta + \mu^{(2)}_{\mathrm{2SS'(a)}}\sin^2\eta) \quad (16)$$

where S, S′ = L, T (with S ≠ S′).

(iii) *Case D.* It is not difficult to see that the second-order self-energy diagrams with two crossed phonon lines of different polarizations both give the same contribution. Then, it is possible to write the added result as

$$\Sigma^{2}_{\mathrm{LT(b)}}(k,\eta) = -\alpha_{\mathrm{L}}\alpha_{\mathrm{T}}\hbar\bar{\omega}\xi^{(2)}_{\mathrm{LT(b)}} - \alpha_{\mathrm{L}}\alpha_{\mathrm{T}}\frac{\hbar^2k^2}{2m^*}(\mu^{(2)}_{\mathrm{1LT(b)}}\cos^2\eta + \mu^{(2)}_{\mathrm{2LT(b)}}\sin^2\eta). \quad (17)$$

In this, and all of the previous cases, the expressions for the $\xi^{(2)}$- and $\mu^{(2)}$-coefficients are explicitly given in the appendix. It is worth noting that the second-order mass correction terms have the same η-dependence as the first-order ones, thus providing the possibility of describing

the effective-mass anisotropy in a homogeneous way. Finally, the second-order correction to the polaron binding energy will be given by

$$\varepsilon_{\mathrm{p}}^{(2)} = -\sum_{\mathrm{S=L,T}} \alpha_{\mathrm{S}}^2(\xi_{\mathrm{S(a)}}^{(2)} + \xi_{\mathrm{S(b)}}^{(2)})\bar{\hbar}\omega_{\mathrm{S}} - \alpha_{\mathrm{L}}\alpha_{\mathrm{T}}(\xi_{\mathrm{LT(a)}}^{(2)} + \xi_{\mathrm{TL(a)}}^{(2)} + \xi_{\mathrm{LT(b)}}^{(2)})\bar{\hbar}\bar{\omega} \tag{18}$$

while the effective-mass correction corresponding to the second order is

$$\begin{aligned}\mu_{\mathrm{p}}^{(2)}(\eta) = &\left(\sum_{\mathrm{S=L,T}} \alpha_{\mathrm{S}}^2(\mu_{\mathrm{1S(a)}}^{(2)} + \mu_{\mathrm{1S(b)}}^{(2)}) + \alpha_{\mathrm{L}}\alpha_{\mathrm{T}}(\mu_{\mathrm{1LT(a)}}^{(2)} + \mu_{\mathrm{1TL(a)}}^{(2)} + \mu_{\mathrm{1LT(b)}}^{(2)})\right)\cos^2\eta \\ &+ \left(\sum_{\mathrm{S=L,T}} \alpha_{\mathrm{S}}^2(\mu_{\mathrm{2S(a)}}^{(2)} + \mu_{\mathrm{2S(b)}}^{(2)}) + \alpha_{\mathrm{L}}\alpha_{\mathrm{T}}(\mu_{\mathrm{2LT(a)}}^{(2)} + \mu_{\mathrm{2TL(a)}}^{(2)} + \mu_{\mathrm{2LT(b)}}^{(2)})\right)\sin^2\eta.\end{aligned} \tag{19}$$

4. Results and discussion

The values for the different parameters involved in the numerical evaluation are listed in table 1. Two different wurtzite nitride materials have been considered: GaN and AlN. The phonon frequencies and dielectric constants have been taken from Azuhata *et al* (1995), Perlin *et al* (1993), and references therein. For GaN, the electron effective mass has been recently measured using different techniques (Drechsler *et al* 1995, Elhamri *et al* 1998). We have chosen the value $m^* = 0.18m_0$ for our spherical GaN effective mass, because it coincides with an experimental (Elhamri *et al* 1998) and calculated average results (Chuang and Chang 1996, Yeo *et al* 1998, Kim and Han 1998) reported recently. For AlN, calculated values of $m_\perp^* = 0.18m_0$ and $m_z^* = 0.25m_0$ are reported (Kim and Han 1998). No definitive experimental value seems to be available for the electron effective mass in this material, and different values have been used in the literature (Chin *et al* 1994, Maeda *et al* 1998). In this case, according to the assumption that we have made, an average value $m^* = 0.22m_0$ has been taken as the input parameter for this material. Nevertheless, as can be seen from the corresponding expressions, the dimensionless ξ- and μ-coefficients are independent of which value is chosen for m^*. All of the information about this quantity is contained in the coupling constants α_{L} and α_{T}.

Table 1. Fundamental oscillation frequencies, dielectric constants, and electronic effective masses for GaN and AlN used in this work.

	Material	
	GaN[a]	AlN[b]
$\omega_\perp$ (cm^{-1})	561	673
ω_z (cm^{-1})	533	660
$\omega_{\perp\mathrm{L}}$ (cm^{-1})	743	916
$\omega_{z\mathrm{L}}$ (cm^{-1})	735	893
$\epsilon_\perp^0$	9.28	8.67
ϵ_z^0	10.01	8.57
$\epsilon_\perp^\infty$	5.29	4.68
m^*/m_0	0.18	0.22[c]

[a] Azuhata *et al* (1995).
[b] Perlin *et al* (1993).
[c] See the text.

In table 2, the parameters defined in this work in order to describe the electron–phonon interaction are presented for both materials, and the numerical results for the dimensionless ξ- and μ-factors in the first and second perturbative orders are then given in tables 3 and 4, respectively. It can be observed, for instance, that the first- and second-order coefficients corresponding to pure LO-like interaction are very close in value for both GaN and AlN, while they differ appreciably in the case of pure TO-like and LO-like-plus-TO-like corrections.

Table 2. Calculated values of the parameters introduced to describe the LO-like and TO-like electron–phonon interactions.

	Material	
	GaN	AlN
$\hbar\omega_{\mathrm{L}}$ (meV)	91.64	112.18
$\hbar\omega_{\mathrm{T}}$ (meV)	67.86	82.66
$\hbar\bar{\omega}$ (meV)	78.85	96.28
α_{L}	0.37	0.42
α_{T}	0.43	0.50
ρ_{L} (Å)	15.66	12.79
ρ_{T} (Å)	21.15	17.36

Table 3. Dimensionless coefficients of the polaronic corrections to the binding energy in the first and second perturbative orders.

	Material	
	GaN	AlN
$\xi_{\mathrm{L}}^{(1)}$	9.85×10^{-1}	1.004
$\xi_{\mathrm{T}}^{(1)}$	3.78×10^{-3}	5.31×10^{-4}
$\xi_{\mathrm{L(a)}}^{(2)}$	6.35×10^{-1}	6.46×10^{-1}
$\xi_{\mathrm{L(b)}}^{(2)}$	3.68×10^{-1}	3.74×10^{-1}
$\xi_{\mathrm{T(a)}}^{(2)}$	8.65×10^{-6}	1.69×10^{-7}
$\xi_{\mathrm{T(b)}}^{(2)}$	5.04×10^{-6}	9.86×10^{-8}
$\xi_{\mathrm{LT(a)}}^{(2)}$	1.92×10^{-3}	2.69×10^{-4}
$\xi_{\mathrm{TL(a)}}^{(2)}$	2.82×10^{-3}	4.03×10^{-4}
$\xi_{\mathrm{LT(b)}}^{(2)}$	1.41×10^{-3}	1.97×10^{-4}

Numerical values for the first- and second-order corrections for the polaron binding energies in GaN and AlN are given in table 5, where the contributions coming from the LO-like, TO-like, and crossed LO–TO phonons have been given separately. The pure TO contributions to the first- and second-order corrections are negligible. However, the crossed term, although smaller than the pure LO contribution, must necessarily be included in order to correctly describe the polaron binding energy. According to table 3, the leading values, coming from the LO-like terms, are very similar for both materials, and what makes the difference between them when evaluating these energy corrections is the value of the coupling constant α_{L}.

With the use of equations (10), (11), and (19), numerical values of the polaron effective mass for limiting values of η: $\eta = 0$ ($m_{\mathrm{p}z}$) and $\eta = \pi/2$ ($m_{\mathrm{p}\perp}$), can be readily calculated. It

Table 4. Dimensionless coefficients of the polaronic corrections to the effective mass in the first and second perturbative orders.

	Material	
	GaN	AlN
$\mu^{(1)}_{1L}$	1.68×10^{-1}	1.66×10^{-1}
$\mu^{(1)}_{2L}$	1.62×10^{-1}	1.67×10^{-1}
$\mu^{(1)}_{1T}$	8.08×10^{-4}	1.12×10^{-4}
$\mu^{(1)}_{2T}$	5.46×10^{-4}	7.67×10^{-5}
$\mu^{(2)}_{1L(a)}$	3.73×10^{-1}	3.01×10^{-1}
$\mu^{(2)}_{1L(b)}$	2.78×10^{-1}	2.76×10^{-1}
$\mu^{(2)}_{2L(a)}$	1.11×10^{-1}	1.15×10^{-1}
$\mu^{(2)}_{2L(b)}$	5.57×10^{-2}	5.72×10^{-2}
$\mu^{(2)}_{1T(a)}$	5.09×10^{-6}	7.75×10^{-8}
$\mu^{(2)}_{1T(b)}$	3.86×10^{-6}	7.51×10^{-8}
$\mu^{(2)}_{2T(a)}$	1.54×10^{-6}	3.02×10^{-8}
$\mu^{(2)}_{2T(b)}$	6.63×10^{-7}	1.82×10^{-8}
$\mu^{(2)}_{1LT(a)}$	8.13×10^{-4}	1.11×10^{-4}
$\mu^{(2)}_{2LT(a)}$	2.94×10^{-4}	4.18×10^{-5}
$\mu^{(2)}_{1TL(a)}$	1.46×10^{-3}	2.08×10^{-4}
$\mu^{(2)}_{2TL(a)}$	5.78×10^{-4}	8.26×10^{-5}
$\mu^{(2)}_{1LT(b)}$	1.04×10^{-3}	1.43×10^{-4}
$\mu^{(2)}_{2LT(b)}$	1.98×10^{-4}	2.78×10^{-5}

Table 5. First- and second-order corrections to the polaron binding energy for GaN and AlN. $\varepsilon^{(1)}_{p,S}$ ($\varepsilon^{(2)}_{p,S}$)—with S = L, T—is the first- (second-) order contribution from the LO and TO optical phonons; $\varepsilon^{(2)}_{p,LT}$ is the crossed LO and TO contribution. $\varepsilon^{(1)}_{p}$ ($\varepsilon^{(2)}_{p}$) is the total first- (second-) order correction.

	Material	
	GaN	AlN
$\varepsilon^{(1)}_{p,L}$ (meV)	-33.4	-47.58
$\varepsilon^{(1)}_{p,T}$ (meV)	-0.11	-2.7×10^{-3}
$\varepsilon^{(1)}_{p}$ (meV)	-33.51	-47.58
$\varepsilon^{(2)}_{p,L}$ (meV)	-12.55	-20.13
$\varepsilon^{(2)}_{p,T}$ (meV)	-1.71×10^{-4}	-5.54×10^{-6}
$\varepsilon^{(2)}_{p,LT}$ (meV)	-7.76×10^{-2}	-1.76×10^{-2}
$\varepsilon^{(2)}_{p}$ (meV)	-12.63	-20.15

is obtained that, for GaN, $m_{pz} = 0.21m_0$ and $m_{p\perp} = 0.19m_0$, giving, on average, the value $m_p = 0.20m_0$, which coincides with the experimental value (Drechsler *et al* 1995) for the

electron effective mass in that material. For AlN, we have: $m_{\mathrm{p}z} = 0.26m_0$ and $m_{\mathrm{p}\perp} = 0.24m_0$, with an average value of $m_{\mathrm{p}} = 0.25m_0$.

The first- and second-order effective-mass corrections are shown in figure 2 for GaN and in figure 3 for AlN. As can be seen, the first-order effective-mass correction is essentially isotropic for both compounds. However, the second-order effective-mass corrections are anisotropic, showing a reduced effect for electrons moving in the xy-plane ($\eta = \pi/2$). The relative magnitude of the effective-mass correction, $M_r = m_{\mathrm{p}}(\eta)/m^* - 1$, versus η (figures 2(b) and 3(b)), is shown as well. The relative difference $1 - M_r(\pi/2)/M_r(0)$ gives a value of 0.49 for GaN and 0.41 for AlN. Thus, the angular variation of M_r is 51% and 59%, respectively, from $\eta = 0$ to $\eta = \pi/2$. This result is significantly different to that previously reported by the authors (Mora-Ramos *et al* 1999), where a very small anisotropy effect in the polaron effective mass was reported for GaN when taking into account only the first-order corrections.

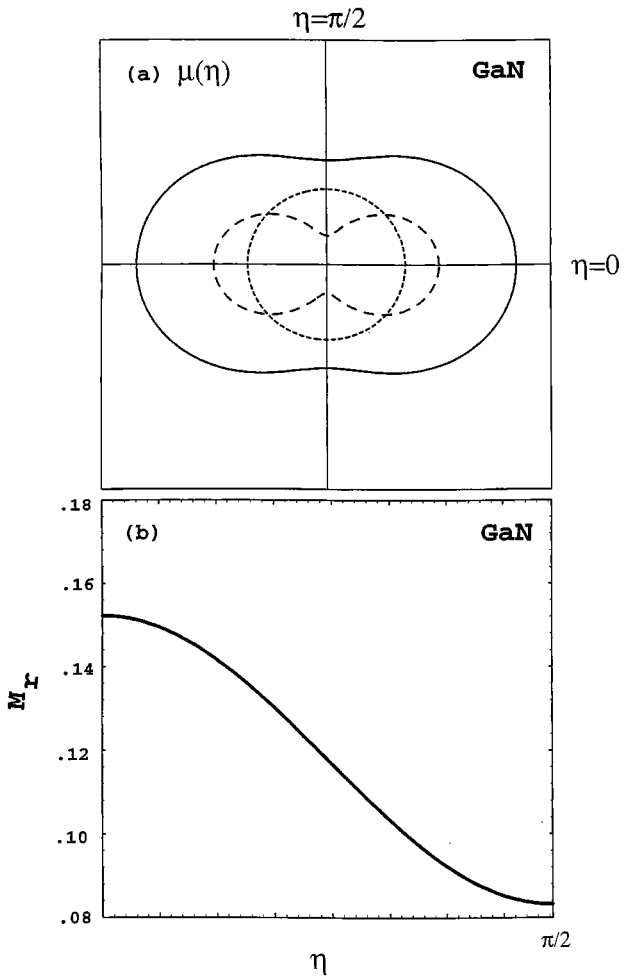

Figure 2. The GaN polaronic mass. (a) The mass renormalization factor $\mu(\eta)$. The dotted line represents the first-order corrections, the dashed line second-order corrections, and the solid line the total correction. (b) The relative magnitude of the effective-mass correction as a function of η, the angle between the electron wavevector and the z-axis of the wurtzite crystalline structure.

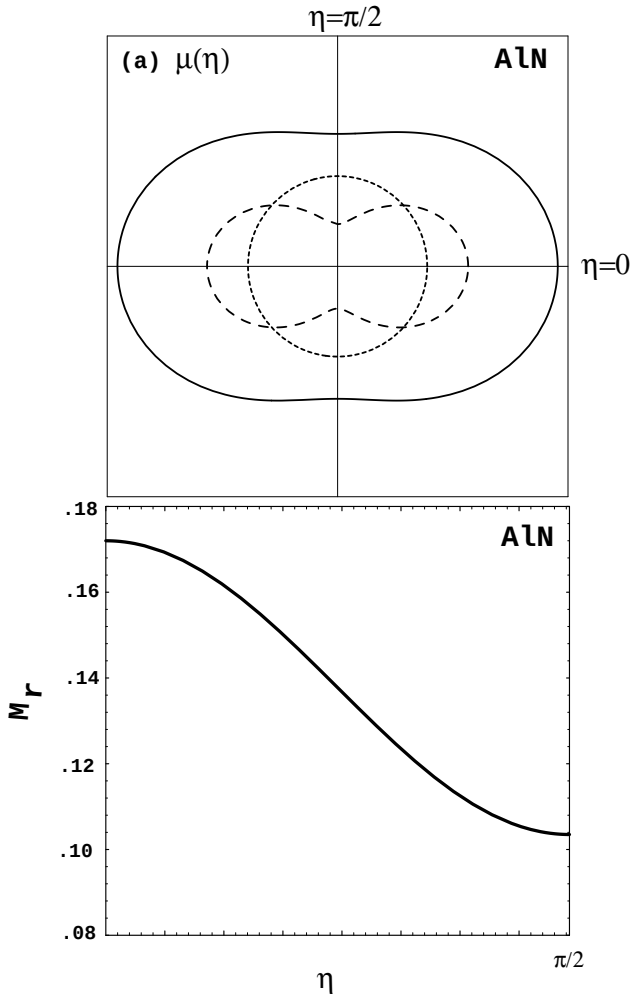

Figure 3. As figure 2, but for AlN.

The use of a more realistic model for the conduction band electronic states, with the inclusion of different unperturbed values for the effective masses along the z-direction and in the xy-plane, should lead to a complete description of this effect, and will be published elsewhere. However, even within the spherically symmetric approximation for the electron effective mass, an important anisotropy effect is found.

5. Conclusions

We have reported in this work the calculation of the polaron binding energy and effective mass up to second-order perturbation theory for wurtzite materials with the use of a recently proposed DCM electron–phonon Hamiltonian. This is done in the framework of the standard Rayleigh–Schrödinger perturbation theory, which is the usual perturbative method in the case of weak electron–phonon coupling. The different feature here is introduced by the inherent anisotropy of the wurtzite structure. This is reflected in the interaction Hamiltonian in such a

way that no general expression for the perturbative expansion in the coupling constants like that in the isotropic Fröhlich bulk case can be given (Mahan 1990). Here, the existence of an angular dispersion in the phonon frequencies makes the calculation process more complicated than in the situation where Einstein phonons (Mahan 1990) or acoustic ones—with linear dispersion—are considered (Woods and Mahan 1998). Thus, in the present model, the coefficients of the expansion have to be evaluated for each wurtzite material.

Numerical values for the cases of GaN and AlN show that the magnitude of the coupling between the conduction electrons and the infrared-active polar optical phonons obtained within the model is large enough to provide significant polaronic corrections, thus justifying the assertion of the need for their evaluation. The magnitude of the polaron binding energy should manifest itself in optical experiments, for instance. Furthermore, an important anisotropy in the effective mass is reported even when a non-perturbed spherically symmetric value is used as input parameter. Both LO-like and TO-like oscillation modes contribute, although the relative weight of the TO-like contribution is much smaller than that of the one coming from the LO-like phonons. In the present work it has been shown that the second-order corrections coming from the self-energy diagrams with phonon lines of different polarization are important for appropriately describing the effective-mass anisotropy. The effect of the carrier–phonon interaction on the electronic mass anisotropy must be of importance when studying, for instance, transport properties in this kind of system. It is worth noting that the inclusion of the electron–phonon correction in the unperturbed theoretical value of the GaN effective mass obtained through electronic structure calculations leads in our work to the reproduction of the experimental value obtained through cyclotron resonance measurements (Drechsler *et al* 1995). Our value is also within the experimental range: $m^* = (0.18 \pm 0.02)m_0$ (Elhamri *et al* 1998) for the same material.

From the results presented, it is seen that making the second-order corrections is definitely unavoidable, especially if a numerical value for the polaron effective mass is looked for. Contributions to this magnitude coming from the second-order terms in the self-energy are of the same order of magnitude as the first-order ones. In the case of the binding energy, these terms also provide a significant contribution, but it is in fact smaller than the corresponding first-order values, as expected.

In both materials, the contributions coming from the pure TO-like terms could be neglected, even in the first perturbative order, as is obviously appropriate for AlN. Nonetheless, the second-order diagrams with mixed polarization lines provide values two to four orders of magnitude higher than the pure TO-like second-order terms leading, in the case of GaN—where the TO-like values have a greater relative weight in the total magnitude—to non-negligible contributions. In contrast, for AlN, it is a very good approximation to deal only with the LO-like electron–phonon interaction when calculating the polaronic corrections. The situation might be different for other wurtzite materials, where the relative contribution of the TO-like modes to the strength of the electron–phonon interaction could be appreciable.

The magnitude of the polaron mass anisotropy can also be related to some material factors like the phonon frequencies and dielectric constant. Then, wurtzite semiconductors like II–VI compounds, which have larger ionicities but similar phonon frequencies, should present a larger polaron mass anisotropy, which could be calculated in the same way as described here, but experimental Fröhlich constants for these materials are scarce (even for InN, available data on the phonon frequencies and dielectric constants are not complete). It can be expected that for different wurtzite materials, a higher influence of the electron–phonon interaction on the effective-mass anisotropy could have appreciable results.

We can expect appreciable contributions from these electron–phonon interaction processes at room temperature. It has already been reported that there is an increase of one order of

magnitude in the polaron damping rates on going from $T = 100$ K to $T = 300$ K, for both first-order LO-like and first-order TO-like processes (Mora-Ramos *et al* 1999). Considering the results of the present calculation, we can infer a similar behaviour in the strength of the second-order mixed-polarization scattering events. The values obtained for the polaron binding energies indicate the importance that the carrier–phonon interaction might have—for instance, in the study of exciton-related optical processes in wurtzite semiconducting materials and heterostructures based on them. It is very well known that these materials have interesting applications in optoelectronics; e.g. III–V nitride-based blue-green semiconductor lasers have already been produced.

Acknowledgments

MEMR is grateful for kind hospitality from the Department of Physics, University of Los Andes, where this work was initiated. FJR and LQ acknowledge support from COLCIENCIAS.

Appendix

The expressions for the contributions coming from first- and second-order diagrams to the polaron self-energy are given in this appendix. For cases A and B, $\xi^{(2)}_{\mathrm{S(a)}}$, $\mu^{(2)}_{\mathrm{1S(a)}}$, and $\mu^{(2)}_{\mathrm{2S(a)}}$ in equation (14) are given by

$$\xi^{(2)}_{\mathrm{S(a)}} = \frac{2}{\pi^3}\frac{\epsilon^*_z\epsilon^*_\perp}{\omega^2_{\mathrm{S}}}\int_0^\infty \mathrm{d}y\int_0^\infty \mathrm{d}z\int_{-1}^1 \frac{\mathrm{d}w}{\sqrt{1-w^2}}\int_{-1}^1 \mathrm{d}x_1\,\frac{f_{\mathrm{S}}(x_1)}{\Omega_{\mathrm{S}}(x_1)}\int_{-1}^1 \mathrm{d}x_2\,\frac{f_{\mathrm{S}}(x_2)}{\Omega_{\mathrm{S}}(x_2)} \times F^{00}_{21}(x_1, x_2, w, y, z)$$

$$\begin{aligned}\mu^{(2)}_{\mathrm{1S(a)}} = {} & \frac{8}{\pi^3}\frac{\epsilon^*_z\epsilon^*_\perp}{\omega^2_{\mathrm{S}}}\int_0^\infty \mathrm{d}y\int_0^\infty \mathrm{d}z\int_{-1}^1 \frac{\mathrm{d}w}{\sqrt{1-w^2}}\int_{-1}^1 \mathrm{d}x_1\,\frac{f_{\mathrm{S}}(x_1)}{\Omega_{\mathrm{S}}(x_1)}\int_{-1}^1 \mathrm{d}x_2\,\frac{f_{\mathrm{S}}(x_2)}{\Omega_{\mathrm{S}}(x_2)} \\ & \times [x_1^2(3F^{20}_{41}(x_1, x_2, w, y, z) + 2F^{20}_{32}(x_1, x_2, w, y, z) + F^{20}_{23}(x_1, x_2, w, y, z)) \\ & + x_2^2 F^{02}_{23}(x_1, x_2, w, y, z) + 2x_1x_2(F^{11}_{32}(x_1, x_2, w, y, z) + F^{11}_{23}(x_1, x_2, w, y, z))]\end{aligned}$$

$$\begin{aligned}\mu^{(2)}_{\mathrm{2S(a)}} = {} & \frac{4}{\pi^3}\frac{\epsilon^*_z\epsilon^*_\perp}{\omega^2_{\mathrm{S}}}\int_0^\infty \mathrm{d}y\int_0^\infty \mathrm{d}z\int_{-1}^1 \frac{\mathrm{d}w}{\sqrt{1-w^2}}\int_{-1}^1 \mathrm{d}x_1\,\frac{f_{\mathrm{S}}(x_1)}{\Omega_{\mathrm{S}}(x_1)}\int_{-1}^1 \mathrm{d}x_2\,\frac{f_{\mathrm{S}}(x_2)}{\Omega_{\mathrm{S}}(x_2)} \\ & \times \Big[(1-x_1^2)(3F^{20}_{41}(x_1, x_2, w, y, z) + 2F^{20}_{32}(x_1, x_2, w, y, z) \\ & + F^{20}_{23}(x_1, x_2, w, y, z)) + (1-x_2^2)F^{02}_{23}(x_1, x_2, w, y, z) \\ & - 2\sqrt{(1-x_1^2)(1-x_2^2)}(F^{11}_{32}(x_1, x_2, w, y, z) + F^{11}_{23}(x_1, x_2, w, y, z))\Big]\end{aligned}$$

with the F-functions given by

$$F^{kl}_{mn}(x_1, x_2, w, y, z) = \frac{y^k}{(y^2 + \Omega_{\mathrm{S}}(x_1)/\omega_{\mathrm{S}})^m}\,\frac{z^l}{(z^2 + y^2 + 2yz\cos\vartheta + [\Omega_{\mathrm{S}}(x_1) + \Omega_{\mathrm{S}}(x_2)]/\omega_{\mathrm{S}})^n}.$$

For cases A and B, the contributions of the diagrams in figure 1(b), $\xi^{(2)}_{\mathrm{S(b)}}$, $\mu^{(2)}_{\mathrm{1S(b)}}$, and $\mu^{(2)}_{\mathrm{2S(b)}}$, in equation (15) are

$$\xi^{(2)}_{\mathrm{S(b)}} = \frac{2}{\pi^3}\frac{\epsilon^*_z\epsilon^*_\perp}{\omega^2_{\mathrm{S}}}\int_0^\infty \mathrm{d}y\int_0^\infty \mathrm{d}z\int_{-1}^1 \frac{\mathrm{d}w}{\sqrt{1-w^2}}\int_{-1}^1 \mathrm{d}x_1\,\frac{f_{\mathrm{S}}(x_1)}{\Omega_{\mathrm{S}}(x_1)}\int_{-1}^1 \mathrm{d}x_2\,\frac{f_{\mathrm{S}}(x_2)}{\Omega_{\mathrm{S}}(x_2)} \times G^{00}_{111}(x_1, x_2, w, y, z)$$

$$\mu^{(2)}_{1\mathrm{S(b)}} = \frac{8}{\pi^3}\frac{\epsilon^*_z\epsilon^*_\perp}{\omega^2_\mathrm{S}}\int_0^\infty \mathrm{d}y\int_0^\infty \mathrm{d}z\int_{-1}^{1}\frac{\mathrm{d}w}{\sqrt{1-w^2}}\int_{-1}^{1}\mathrm{d}x_1\,\frac{f_\mathrm{S}(x_1)}{\Omega_\mathrm{S}(x_1)}\int_{-1}^{1}\mathrm{d}x_2\,\frac{f_\mathrm{S}(x_2)}{\Omega_\mathrm{S}(x_2)}$$
$$\times [x_1^2(G^{20}_{311}(x_1,x_2,w,y,z)+G^{20}_{212}(x_1,x_2,w,y,z)+G^{20}_{113}(x_1,x_2,w,y,z))$$
$$+ x_2^2(G^{02}_{131}(x_1,x_2,w,y,z)+G^{02}_{122}(x_1,x_2,w,y,z)+G^{02}_{113}(x_1,x_2,w,y,z))$$
$$+ x_1x_2(G^{11}_{221}(x_1,x_2,w,y,z)+G^{11}_{212}(x_1,x_2,w,y,z)+G^{11}_{122}(x_1,x_2,w,y,z)$$
$$+ 2G^{11}_{113}(x_1,x_2,w,y,z))]$$

$$\mu^{(2)}_{2\mathrm{S(b)}} = \frac{4}{\pi^3}\frac{\epsilon^*_z\epsilon^*_\perp}{\omega^2_\mathrm{S}}\int_0^\infty \mathrm{d}y\int_0^\infty \mathrm{d}z\int_{-1}^{1}\frac{\mathrm{d}w}{\sqrt{1-w^2}}\int_{-1}^{1}\mathrm{d}x_1\,\frac{f_\mathrm{S}(x_1)}{\Omega_\mathrm{S}(x_1)}\int_{-1}^{1}\mathrm{d}x_2\,\frac{f_\mathrm{S}(x_2)}{\Omega_\mathrm{S}(x_2)}$$
$$\times\Big[(1-x_1^2)(G^{20}_{311}(x_1,x_2,w,y,z)+G^{20}_{212}(x_1,x_2,w,y,z)$$
$$+ G^{20}_{113}(x_1,x_2,w,y,z))+(1-x_2^2)(G^{02}_{131}(x_1,x_2,w,y,z)$$
$$+ G^{02}_{122}(x_1,x_2,w,y,z)+G^{02}_{113}(x_1,x_2,w,y,z))$$
$$-\sqrt{(1-x_1^2)(1-x_2^2)}(G^{11}_{221}(x_1,x_2,w,y,z)+G^{11}_{212}(x_1,x_2,w,y,z)$$
$$+ G^{11}_{122}(x_1,x_2,w,y,z)+2G^{11}_{113}(x_1,x_2,w,y,z))\Big].$$

In this case, the G-functions are defined as

$$G^{kl}_{mnr}(x_1,x_2,w,y,z) = \frac{y^k}{(y^2+\Omega_\mathrm{S}(x_1)/\omega_\mathrm{S})^m}\frac{z^l}{(z^2+\Omega_\mathrm{S}(x_2)/\omega_\mathrm{S})^n}$$
$$\times\frac{1}{(z^2+y^2+2yz\cos\vartheta+[\Omega_\mathrm{S}(x_1)+\Omega_\mathrm{S}(x_2)]/\omega_\mathrm{S})^r}.$$

The contributions coming from diagrams with phonon lines of different polarizations, $\xi^{(2)}_{\mathrm{SS'(a)}}$, $\mu^{(2)}_{1\mathrm{SS'(a)}}$, and $\mu^{(2)}_{2\mathrm{SS'(a)}}$, with S, S′ = L, T and S ≠ S′, as appropriate for case C, in equation (16) are the following:

$$\xi^{(2)}_{\mathrm{SS'(a)}} = \frac{2}{\pi^3}\frac{\epsilon^*_z\epsilon^*_\perp}{\bar\omega^2}\int_0^\infty \mathrm{d}y\int_0^\infty \mathrm{d}z\int_{-1}^{1}\frac{\mathrm{d}w}{\sqrt{1-w^2}}\int_{-1}^{1}\mathrm{d}x_1\,\frac{f_\mathrm{S}(x_1)}{\Omega_\mathrm{S}(x_1)}\int_{-1}^{1}\mathrm{d}x_2\,\frac{f_{\mathrm{S'}}(x_2)}{\Omega_{\mathrm{S'}}(x_2)}$$
$$\times\mathcal{F}^{00}_{\mathrm{SS'}21}(x_1,x_2,w,y,z)$$

$$\mu^{(2)}_{1\mathrm{SS'(a)}} = \frac{8}{\pi^3}\frac{\epsilon^*_z\epsilon^*_\perp}{\bar\omega^2}\int_0^\infty \mathrm{d}y\int_0^\infty \mathrm{d}z\int_{-1}^{1}\frac{\mathrm{d}w}{\sqrt{1-w^2}}\int_{-1}^{1}\mathrm{d}x_1\,\frac{f_\mathrm{S}(x_1)}{\Omega_\mathrm{S}(x_1)}\int_{-1}^{1}\mathrm{d}x_2\,\frac{f_{\mathrm{S'}}(x_2)}{\Omega_{\mathrm{S'}}(x_2)}$$
$$\times [x_1^2(3\mathcal{F}^{20}_{\mathrm{SS'}41}(x_1,x_2,w,y,z)+2\mathcal{F}^{20}_{\mathrm{SS'}32}(x_1,x_2,w,y,z)$$
$$+ \mathcal{F}^{20}_{\mathrm{SS'}23}(x_1,x_2,w,y,z))+x_2^2\mathcal{F}^{02}_{\mathrm{SS'}23}(x_1,x_2,w,y,z)$$
$$+ 2x_1x_2(\mathcal{F}^{11}_{\mathrm{SS'}32}(x_1,x_2,w,y,z)+\mathcal{F}^{11}_{\mathrm{SS'}23}(x_1,x_2,w,y,z))]$$

$$\mu^{(2)}_{2\mathrm{SS'(a)}} = \frac{4}{\pi^3}\frac{\epsilon^*_z\epsilon^*_\perp}{\bar\omega^2}\int_0^\infty \mathrm{d}y\int_0^\infty \mathrm{d}z\int_{-1}^{1}\frac{\mathrm{d}w}{\sqrt{1-w^2}}\int_{-1}^{1}\mathrm{d}x_1\,\frac{f_\mathrm{S}(x_1)}{\Omega_\mathrm{S}(x_1)}\int_{-1}^{1}\mathrm{d}x_2\,\frac{f_{\mathrm{S'}}(x_2)}{\Omega_{\mathrm{S'}}(x_2)}$$
$$\times\Big[(1-x_1^2)(3\mathcal{F}^{20}_{\mathrm{SS'}41}(x_1,x_2,w,y,z)+2\mathcal{F}^{20}_{\mathrm{SS'}32}(x_1,x_2,w,y,z)$$
$$+ \mathcal{F}^{20}_{\mathrm{SS'}23}(x_1,x_2,w,y,z))+(1-x_2^2)\mathcal{F}^{02}_{\mathrm{SS'}23}(x_1,x_2,w,y,z)$$
$$-2\sqrt{(1-x_1^2)(1-x_2^2)}(\mathcal{F}^{11}_{\mathrm{SS'}32}(x_1,x_2,w,y,z)+\mathcal{F}^{11}_{\mathrm{SS'}23}(x_1,x_2,w,y,z))\Big]$$

where

$$\mathcal{F}^{kl}_{\mathrm{SS'}mn}(x_1,x_2,w,y,z) = \frac{y^k}{(y^2+\Omega_\mathrm{S}(x_1)/\bar\omega)^m}\frac{z^l}{(z^2+y^2+2yz\cos\vartheta+[\Omega_\mathrm{S}(x_1)+\Omega_{\mathrm{S'}}(x_2)]/\bar\omega)^n}.$$

The contributions coming from crossed diagrams of different polarizations, $\xi^{(2)}_{\mathrm{LT(b)}}$, $\mu^{(2)}_{\mathrm{1LT(b)}}$, and $\mu^{(2)}_{\mathrm{2LT(b)}}$, are then given by

$$\xi^{(2)}_{\mathrm{LT(b)}} = \frac{4}{\pi^3}\frac{\epsilon^*_z\epsilon^*_\perp}{\bar{\omega}^2}\int_0^\infty \mathrm{d}y\int_0^\infty \mathrm{d}z\int_{-1}^1 \frac{\mathrm{d}w}{\sqrt{1-w^2}}\int_{-1}^1 \mathrm{d}x_1\,\frac{f_{\mathrm{L}}(x_1)}{\Omega_{\mathrm{L}}(x_1)}\int_{-1}^1 \mathrm{d}x_2\,\frac{f_{\mathrm{T}}(x_2)}{\Omega_{\mathrm{T}}(x_2)} \times \mathcal{G}^{00}_{111}(x_1, x_2, w, y, z)$$

$$\begin{aligned}\mu^{(2)}_{\mathrm{1LT(b)}} = \frac{16}{\pi^3}\frac{\epsilon^*_z\epsilon^*_\perp}{\bar{\omega}^2}\int_0^\infty \mathrm{d}y\int_0^\infty \mathrm{d}z\int_{-1}^1 \frac{\mathrm{d}w}{\sqrt{1-w^2}}\int_{-1}^1 \mathrm{d}x_1\,\frac{f_{\mathrm{L}}(x_1)}{\Omega_{\mathrm{L}}(x_1)}\int_{-1}^1 \mathrm{d}x_2\,\frac{f_{\mathrm{T}}(x_2)}{\Omega_{\mathrm{T}}(x_2)}\\ \times [x_1^2(\mathcal{G}^{20}_{311}(x_1, x_2, w, y, z) + \mathcal{G}^{20}_{212}(x_1, x_2, w, y, z) + \mathcal{G}^{20}_{113}(x_1, x_2, w, y, z))\\ + x_2^2(\mathcal{G}^{02}_{131}(x_1, x_2, w, y, z) + \mathcal{G}^{02}_{122}(x_1, x_2, w, y, z) + \mathcal{G}^{02}_{113}(x_1, x_2, w, y, z))\\ + x_1x_2(\mathcal{G}^{11}_{221}(x_1, x_2, w, y, z) + \mathcal{G}^{11}_{212}(x_1, x_2, w, y, z) + \mathcal{G}^{11}_{122}(x_1, x_2, w, y, z)\\ + 2\mathcal{G}^{11}_{113}(x_1, x_2, w, y, z))]\end{aligned}$$

$$\begin{aligned}\mu^{(2)}_{\mathrm{2LT(b)}} = \frac{8}{\pi^3}\frac{\epsilon^*_z\epsilon^*_\perp}{\bar{\omega}^2}\int_0^\infty \mathrm{d}y\int_0^\infty \mathrm{d}z\int_{-1}^1 \frac{\mathrm{d}w}{\sqrt{1-w^2}}\int_{-1}^1 \mathrm{d}x_1\,\frac{f_{\mathrm{L}}(x_1)}{\Omega_{\mathrm{L}}(x_1)}\int_{-1}^1 \mathrm{d}x_2\,\frac{f_{\mathrm{T}}(x_2)}{\Omega_{\mathrm{T}}(x_2)}\\ \times \Big[(1-x_1^2)(\mathcal{G}^{20}_{311}(x_1, x_2, w, y, z) + \mathcal{G}^{20}_{212}(x_1, x_2, w, y, z)\\ + \mathcal{G}^{20}_{113}(x_1, x_2, w, y, z)) + (1-x_2^2)(\mathcal{G}^{02}_{131}(x_1, x_2, w, y, z)\\ + \mathcal{G}^{02}_{122}(x_1, x_2, w, y, z) + \mathcal{G}^{02}_{113}(x_1, x_2, w, y, z))\\ - \sqrt{(1-x_1^2)(1-x_2^2)}(\mathcal{G}^{11}_{221}(x_1, x_2, w, y, z) + \mathcal{G}^{11}_{212}(x_1, x_2, w, y, z)\\ + \mathcal{G}^{11}_{122}(x_1, x_2, w, y, z) + 2\mathcal{G}^{11}_{113}(x_1, x_2, w, y, z))\Big].\end{aligned}$$

The $\mathcal{G}$-functions are

$$\mathcal{G}^{kl}_{mnr}(x_1, x_2, w, y, z) = \frac{y^k}{(y^2 + \Omega_{\mathrm{L}}(x_1)/\bar{\omega})^m}\frac{z^l}{(z^2 + \Omega_{\mathrm{T}}(x_2)/\bar{\omega})^n} \times \frac{1}{(z^2 + y^2 + 2yz\cos\vartheta + [\Omega_{\mathrm{L}}(x_1) + \Omega_{\mathrm{T}}(x_2)]/\bar{\omega})^r}.$$

In all of these equations, the variables y and z, derived from the phonon wavevector magnitudes, have been introduced, as well as the variables $x_1 = \cos\theta_1$ and $x_2 = \cos\theta_2$. θ_1 and θ_2 are the angles between the phonon wavevectors $\boldsymbol{q}_1$ and $\boldsymbol{q}_2$ and the z-axis, respectively. The cosine of the angle between the two wavevectors is a function of the variables x_1 and x_2 and of the angular variables φ_1 and φ_2, the polar angles associated, respectively, with $\boldsymbol{q}_1$ and $\boldsymbol{q}_2$:

$$\cos\vartheta = \cos(\varphi_1 - \varphi_2)\sqrt{(1-x_1^2)(1-x_2^2)} + x_1x_2.$$

As can be seen, the only dependence upon the angular variables φ_1 and φ_2 is given through the argument of the cosine in the last formula. This fact allows us to directly evaluate one of the corresponding polar angular integrals and—what turns out to be the most important consequence—to demonstrate, after straightforward manipulations, that the second-order mass correction terms have the same η-dependence as the first-order ones.

References

Azuhata T, Sota T, Suzuki K and Nakamura S 1995 *J. Phys.: Condens. Matter* **7** L129
Bernardini F, Fiorentini V and Vanderbilt D 1997 *Phys. Rev.* B **56** R10 024

Chin V W L, Tansley T L and Osotchan T 1994 *J. Appl. Phys.* **75** 7365
Chuang S L and Chang C S 1996 *Phys. Rev.* B **54** 2491
Comas F, Pérez-Alvarez R, Trallero-Giner C and Cardona M 1993 *Superlatt. Microstruct.* **14** 95
Comas F, Trallero-Giner C and Cardona M 1997 *Phys. Rev.* B **56** 4115
Davydov A S 1976 *Teoriia Tverdogo Tela* (Moscow: Nauka)
Devreese J T 1996 *Encyclopedia of Applied Physics* vol 14 (Weinheim: VCH) p 886
Drechsler M, Hofmann D M, Meyer B K, Detchprohm T, Amano H and Akasaki I 1995 *Japan. J. Appl. Phys. Suppl.* 1 **34** L1178
Dupuis R D, Edmond J A, Ponce F and Nakamura S (ed) 1996 *Gallium Nitrides and Related Compounds (MRS Symp. Proc. 395)* (Pittsburgh, PA: Materials Research Society)
Elhamri S, Newrock R S, Mat D B, Ahoujja M, Mitchel W C, Redwing J M, Tischler M A and Flynn J S 1998 *Phys. Rev.* B **57** 1374
Fröhlich H 1954 *Adv. Phys.* **3** 325
Khan M A, Kuznia J N, Bhattarai A R and Olson D T 1993 *Appl. Phys. Lett.* **62** 1786
Khan M A, Shur M S, Kuznia J N, Chen Q, Burm J and Schaff W 1995 *Appl. Phys. Lett.* **66** 1083
Kim Ch-H and Han B-H 1998 *Solid State Commun.* **106** 127
Lee B C, Kim K W, Dutta M and Stroscio M A 1997 *Phys. Rev.* B **56** 997
Lee B C, Kim K W, Stroscio M A and Dutta M 1998 *Phys. Rev.* B **58** 4860
Maeda N, Nishida T, Kobayashi N and Tomizawa M 1998 *Appl. Phys. Lett* **73** 1856
Mahan G D 1990 *Many Particle Physics* 2nd edn (New York: Plenum)
Mora-Ramos M E and Contreras-Solorio D A 1998 *Physica* B **253** 325
Mora-Ramos M E, Rodríguez F J and Quiroga L 1999 *Solid State Commun.* **109** 767
Moustakas T D, Pankove J H and Hamakawa Y (ed) 1992 *Wide Band Gap Semiconductors (MRS Symp. Proc. 242)* (Pittsburgh, PA: Materials Research Society)
Nakamura S, Mukai T and Senoh M 1994 *J. Appl. Phys.* **76** 8189
Nakamura S, Senoh M, Nagahama S, Iwasa N, Yamada T, Matsushita T and Kiyoku H 1996 *Appl. Phys. Lett.* **69** 1477
Nakamura S, Senoh M, Nagahama S, Iwasa N, Yamada T, Matsushita T and Kiyoku H 1997 *Appl. Phys. Lett.* **70** 616
O'Leary S K, Foutz B E, Shur M S, Bhapkar U V and Eastman L F 1998 *J. Appl. Phys.* **83** 826
Perlin P, Polian A and Suski T 1993 *Phys. Rev.* B **47** 2874
Ponce F A, Moustakas T D, Asaki I and Monemar B A (ed) 1997 *III–V Nitrides (MRS Symp. Proc. 449)* (Pittsburgh, PA: Materials Research Society)
Ridley B K 1993 *Phys. Rev.* B **47** 4592
Trallero-Giner C, García-Moliner F, Velasco V R and Cardona M 1992 *Phys. Rev.* B **45** 11 944
Van Camp P E, Van Doren V E and Devreese J T 1991 *Phys. Rev.* B **44** 9056
Van Camp P E, Van Doren V E and Devreese J T 1992 *Solid State Commun.* **81** 23
van de Walle C G (ed) 1993 *Proc. 7th Trieste Semiconductor Symp. on Wide-Band-Gap Semiconductors (1992)* (Amsterdam: North-Holland)
Wendler L 1985 *Phys. Status Solidi* b **129** 513
Woods L M and Mahan G D 1998 *Phys. Rev.* B **57** 7679
Yeo Y C, Chong T C and Li M F 1998 *J. Appl. Phys.* **83** 1429